Journal of Alloys and Compounds, 194 (1993) 447–454
JALCOM 7227

Atomistic simulation of radiation-induced amorphization of the ordered compound NiZr

R. Devanathan
Materials Science Division, Argonne National Laboratory, Argonne, IL 60439 (USA)
and Department of Materials Science and Engineering, Northwestern University, Evanston, IL 60208 (USA)

N. Q. Lam and P. R. Okamoto
Materials Science Division, Argonne National Laboratory, Argonne, IL 60439 (USA)

M. J. Sabochick
Computer Applications Division, Gulf States Utilities Co., Beaumont, TX 77704 (USA)

M. Meshii
Department of Materials Science and Engineering, Northwestern University, Evanston, IL 60208 (USA)

(Received February 25, 1992; in final form September 22, 1992)

Abstract

We have investigated the electron-irradiation-induced amorphization of the ordered compound NiZr using molecular dynamics simulations. Ni and Zr atoms were randomly exchanged and Frenkel pairs were introduced, in two separate processes, to simulate the effects of electron irradiation. The interatomic potentials for the simulations were developed using the embedded-atom method. During the simulation, the state of the system was studied by monitoring changes in thermodynamic, mechanical and structural properties as functions of damage dose. Our results indicate that NiZr can be amorphized by atom exchanges as well as by the introduction of Frenkel pairs and are in agreement with experimental observations.

1. Introduction

Crystalline materials can be amorphized in the solid state by a variety of techniques such as irradiation by energetic particles, mechanical alloying, hydrogenation and annealing of multilayer films [1]. Of these, electron-irradiation-induced amorphization has been extensively studied because of the simple nature of the resulting damage [2–12]. The damage produced by electrons basically consists of two defect components, namely isolated interstitials and vacancies (Frenkel pairs) and chemical disorder. In spite of this simplicity, the relative importance of chemical disorder and point defects in the amorphization process has been a subject of considerable debate.

Several experimental studies have been performed to elucidate the mechanism of amorphization of intermetallic compounds. Luzzi *et al.* [2, 3] irradiated Cu_4Ti_3 with 2 MeV electrons and measured the Bragg–Williams long-range order parameter as a function of dose at various temperatures. Below 265 K, they observed considerable chemical disorder followed by a complete crystalline-to-amorphous (CA) transition. Above 265 K, the compound was found to exhibit very little chemical disorder and irradiation merely led to the production of secondary defects. They also found preferential amorphization at antiphase domain boundaries. On the basis of the above evidence and a high resolution electron microscopy study of the CA interface, Luzzi *et al.* have concluded that chemical disordering destabilizes crystalline Cu_4Ti_3 with respect to the amorphous state.

On the contrary, Mori *et al.* [4, 5] irradiated NiTi with 2 MeV electrons in the temperature range 50–393 K and observed preferential amorphization of small islands along dislocation lines. These small amorphous regions grew with increasing dose and ultimately coalesced into one body. These researchers concluded that the accumulation of vacancies produced by electron irradiation plays an essential role in the observed CA transition. The amorphization kinetics in NiTi has been modeled by Pedraza [6]. The model proposes amorphization by the accumulation of vacancy–interstitial complexes that relax local stresses while creating chemical short-range order and local topological disorder.

0925-8388/93/$6.00

Koike *et al.* [7] found that, during 1 MeV electron irradiation, Zr_3Al could be readily amorphized at temperatures below about 15 K, but was only partially amorphized at 57 K, even after a dose of about 43 displacements per atom (DPA). The aggregation of point defects, evidenced by striations in bright field images and diffuse scattering in diffraction patterns, was observed at 57 K. These observations led Koike *et al.* to conclude that the accumulation of point defects is a necessary driving force for complete amorphization in Zr_3Al.

In addition to these experiments, molecular dynamics (MD) simulations have been performed to study the mechanism of amorphization in intermetallic compounds. In contrast to irradiation experiments, simulations provide the opportunity to separate the effects of chemical disorder from those of point defects. Therefore, it is possible to study a particular mechanism in isolation. Sabochick and Lam [8, 9] and Lam *et al.* [10] used embedded-atom potentials to simulate the effects of Frenkel pairs and chemical disorder in the intermetallic compounds of the Cu–Ti and Ni–Ti system. They found that in all three compounds Frenkel pairs were required to bring about amorphization while chemical disorder merely increased the energy of the system. In contrast, Massobrio *et al.* [11] were able to amorphize $NiZr_2$ by introducing chemical disorder in an MD simulation performed with tight-binding potentials.

In an effort to shed more light on the nature of the driving force for amorphization, we have performed, using embedded-atom potentials, a systematic MD simulation of the effects of chemical disorder and Frenkel pairs in three intermetallic compounds of the Ni–Zr system, *i.e.* NiZr, $NiZr_2$ and Ni_3Zr. Complete amorphization, by 1 MeV electron irradiation in the temperature range 10–200 K, has been recently observed in all of these compounds by Xu *et al.* [12]. In the present paper, the simulation results obtained for the compound NiZr are reported.

2. Details of the simulation

2.1. The model system

The MD simulations were performed in an isothermal, isobaric ensemble using a modified version of the DYNAMO computer code [13]. The code was vectorized to achieve optimum performance on the Cray XMP and Cray 2 supercomputers. The compound NiZr has the oC8 structure shown in Fig. 1. The simulation cell was rectangular and consisted of 500 Ni and 500 Zr atoms. It was maintained at a temperature of 30 K and zero pressure. The interatomic potentials were developed using the embedded-atom method as discussed below. Throughout this simulation, a time step of 2×10^{-15} s was used.

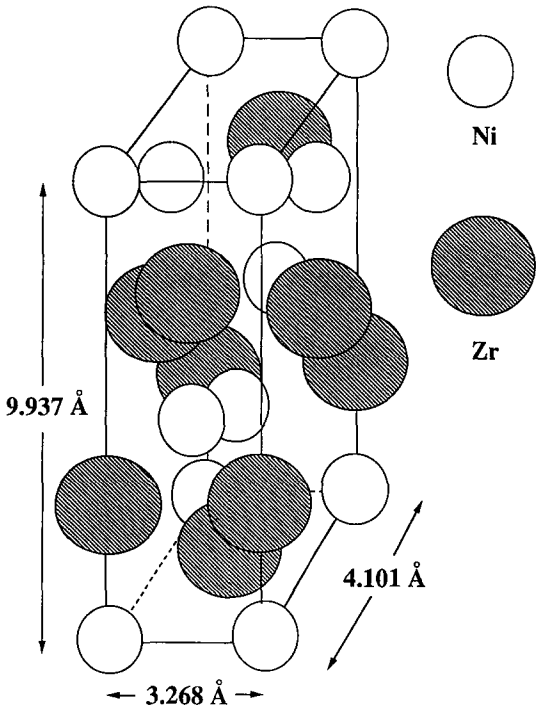

Fig. 1. The ordered structure of NiZr.

The perfect lattice configuration was initially equilibrated for 5000 time steps. The effects of electron irradiation were simulated by introducing chemical disorder and Frenkel pairs in two separate runs. Chemical disorder was produced by exchanging a randomly chosen pair of Ni and Zr atoms every ten time steps. Frenkel pairs were created by removing a randomly chosen atom and re-inserting it at a random position in the cell every ten steps. While inserting the atom in the new position, a minimum separation from other atoms of 0.07 nm was maintained to avoid numerical instabilities. During both the exchange process and the introduction of Frenkel pairs, the configurations corresponding to various doses were saved and subsequently equilibrated for 20 000 time steps. We define the dose as the number of DPA for the case of Frenkel pairs, and as the number of exchanges per atom (EPA) for the case of atom exchanges. Following this equilibration, the potential energy E, volume V, pair correlation function $g(r)$, structure factor $H(k)$ and the shear elastic constants were averaged over 10 000 steps. The state of the system was systematically studied by monitoring, as functions of dose, the changes in the above properties and in the projections of atom positions along the [100] direction. These properties were also compared with those of the perfect crystal and of a quenched liquid. The quench run was carried out by equilibrating the system at 4000 K for 10 000 steps and then changing the temperature to 30 K. The system was then equil-

ibrated at 30 K for 10 000 steps and the properties were averaged over the next 10 000 time steps.

2.2. The embedded-atom potentials

The embedded-atom potentials used in this work were obtained using the method of Oh and Johnson [14]. The basic equations of this method are

$$E(r^N)=\sum_i F_i(\rho_i)+\frac{1}{2}\sum_{i\neq j}\Phi_{ij}(r_{ij}) \quad (1)$$

$$\rho_i=\sum_{i\neq j} f_j(r_{ij}) \quad (2)$$

$$f_j(r_{ij})=f_{e,m}\exp\left[-\beta_m\left(\frac{r_{ij}}{r_{e,mm}}-1\right)\right] \quad (3)$$

$$\Phi_{ij}(r_{ij})=\Phi_{e\,km}\exp\left[-\gamma_{km}\left(\frac{r_{ij}}{r_{e,km}}-1\right)\right]\left\{\exp\left[-\lambda_{km}\left(\frac{r_{ij}}{r_{e,km}}-1\right)\right]-\kappa_{km}\right\} \quad (4)$$

where E is the potential energy of a system of N atoms, F_i is the embedding energy for atom i, ρ_i is the electron density at i due to the other atoms in the system, r_{ij} is the distance separating atoms i and j which belong to the chemical species k and m respectively, r_e is the equilibrium interatomic distance and Φ_{ij} is the two-body potential between atoms i and j. The interactions were smoothly terminated, as discussed by Sabochick and Lam [8], at a cut-off radius $r_{c,km}=s_{c,km}r_{e,km}$. The embedding functions for Ni and Zr were obtained by satisfying the equation of state of Oh and Johnson [14], which is a modification of the equation given by Rose *et al.* [15]:

$$F_k[\rho_k(z)]=-E_{c,k}\left[1+\alpha_k(z-1)\left(\frac{1}{z^{h_k}}-\frac{h_k}{z}+h_k\right)\right]\exp\left[-\alpha_k\left(z-1\right)\right]-\frac{1}{2}\sum_n \Phi_{kk}(zr^n) \quad (5)$$

Here, z is the ratio of the edge length of an expanded or compressed perfect crystal to that of a perfect crystal at zero pressure, α_k is a constant and h_k is a hardening parameter as described by Oh and Johnson [14]. The sum is over all the neighbors n of an atom in a perfect crystal. The electron density $\rho_k(z)$ is given by

$$\rho_k(z)=\sum_n f_k(zr^n) \quad (6)$$

Table 1 lists the parameters of the Ni, Zr and Ni–Zr potentials. These parameters were fitted to the equilibrium properties of the pure metals Ni and Zr and the compounds NiZr, $NiZr_2$ and Ni_3Zr. Table 2 shows the results of the fit to the pure metal properties. The potentials for Ni were obtained from the work of Sabochick and Lam [20]. For Zr, the atomic volume, c/a ratio, elastic constants and the relaxed vacancy formation energy were fitted. A good fit was obtained with a maximum relative difference of around 7% between the present work and experimental values. In addition to this fit, the relative stability of b.c.c., f.c.c. and h.c.p. structures was examined for both Ni and Zr. The most stable structures were f.c.c. for Ni and h.c.p. for Zr.

TABLE 1. Parameters of the Ni, Zr and Ni–Zr potentials

Parameter	Ni	Zr	Ni–Zr
$r_{e,km}$ (nm)	0.2489	0.3231	0.262
$s_{c,km}$	1.933	1.6247	1.634
$f_e(\mathrm{Ni})/f_e(\mathrm{Zr})$			1.0
β_k	5.851291	6.0	
$\Phi_{e,km}$ (eV)	1.396287	0.67107	0.682967
γ_{km}	0.6	7.9185	0.36
λ_{km}	5.574038	0.0	5.117182
κ_{km}	0.763544	0.0	1.431682
$E_{c,k}$ (eV)	4.45[a]	6.25[a]	
α_k	4.983	4.553	
h_k	3.2	3.35	

[a]Ref. 16.

The results of the fit to the properties of the three compounds are shown in Table 3. For NiZr and $NiZr_2$, the lattice parameters and the heats of formation were fitted. For Ni_3Zr, the heat of formation was not known, and so only the lattice constants were fitted. The fit to NiZr was within 11% of the experimental values. A good fit was also obtained for the lattice constants of Ni_3Zr and $NiZr_2$. The elastic constants C_{11}, C_{12}, C_{13} and C_{33} of $NiZr_2$ were also calculated and found to be within 20% of the corresponding experimental values [24]. The stability of these lattices (oC8 for NiZr, tI12 for $NiZr_2$ and hP8 for Ni_3Zr) was confirmed by comparing them with the B2 structure for NiZr, $C15_b$ structure for $NiZr_2$ and the $L1_2$ structure for Ni_3Zr.

We have also determined the melting point of NiZr to examine the ability of our potential to model the thermodynamic properties of the system. The system was maintained at various temperatures for 10 000 steps and the potential energy E/N per atom, volume V/N per atom and mean-square displacement $\langle u^2\rangle$ were calculated as functions of temperature. The results are shown in Fig. 2. Both the potential energy and volume increase almost linearly with temperature up to about 1400 K, where an abrupt increase is observed. $\langle u^2\rangle$ attained values characteristic of a liquid at 1450 K. The melting point is, therefore, taken to lie between 1400 K and 1450 K. The experimental melting point is 1533 K [25]. From the plot of volume as a function of temperature, we obtained a value of about 2×10^{-5}

TABLE 2. Results of the fit to the properties of pure Ni and Zr

Property[a]	Ni		Zr	
	Experiment	Present work	Experiment	Present work
Ω ($\times 10^{-3}$ nm^3)	10.90[b]	10.90	23.27[b]	23.27
E_v^f (eV)	1.80[c]	1.80	1.35[d]	1.306
B (Mbar)	1.804[e]	1.798		
G (Mbar)	0.947[e]	0.947		
A	2.51[e]	2.51		
C_{11} (Mbar)			1.554[e]	1.659
C_{12} (Mbar)			0.671[e]	0.719
C_{13} (Mbar)			0.646[e]	0.616
C_{33} (Mbar)			1.730[e]	1.698
C_{44} (Mbar)			0.364[e]	0.365
c/a			1.593[b]	1.623

[a]Ω is the atomic volume, B and G are the bulk and shear moduli, C_{11}, C_{12}, C_{13}, C_{33} and C_{44} are the elastic constants, and E_v^f is the relaxed vacancy formation energy. $A = 2C_{44}/(C_{11}-C_{12})$ is the anisotropy ratio.
[b]Ref. 17.
[c]Ref. 18.
[d]Ref. 14.
[e]Ref. 19.

TABLE 3. Results of the potential fits to the properties of NiZr, $NiZr_2$ and Ni_3Zr

Property[a]	NiZr		$NiZr_2$		Ni_3Zr	
	Experiment	Present work	Experiment	Present work	Experiment	Present work
a (nm)	0.3268[b]	0.3131	0.6483[b]	0.6378	0.5309[c]	0.5273
b (nm)	0.9937[b]	1.0106				
c (nm)	0.4101[b]	0.4003	0.5267[b]	0.5184	0.4303[c]	0.4166
ΔH^f (eV atom^{-1})	0.267[d]	0.300	0.127[d]	0.240		0.337

[a]a, b and c are the lattice parameters and H^f is the heat of formation.
[b]Ref. 21.
[c]Ref. 22.
[d]Ref. 23.

K^{-1} for the coefficient of linear thermal expansion. At 1400 K, the diffusion coefficient attained a value of about 2.5×10^{-5} cm^2 s^{-1}. Both the value of the diffusion coefficient near the melting point and the linear behavior of the thermodynamic properties below the melting point are consistent with the results of Massobrio *et al.* [11] for $NiZr_2$. A note of explanation about the calculation of $\langle u^2 \rangle$ is in order here. We have calculated the value of $\langle u^2 \rangle$ averaged along the x, y and z directions in the present work, while Massobrio *et al.* have calculated $\langle u^2 \rangle$ along the x direction in $NiZr_2$. This fact should be taken into account while comparing these two results.

3. Results and discussion

3.1. Thermodynamic properties

The energy and volume of the system are two thermodynamic properties that are easy to monitor in a simulation. Figure 3 shows the change in the potential energy and volume expansion as a function of dose. It can be seen that these quantities increase monotonically with dose and reach the level of the quenched liquid at about 0.2 DPA for the case of Frenkel pairs and at about 0.2 EPA for exchanges. When the dose is increased beyond this level, the energy and volume tend to saturate. The fact that the energy and volume of the system have risen above the corresponding quantities of the quenched liquid indicates that the system might be amorphized by both Frenkel pairs and chemical disorder. In order to investigate this possibility, we studied the structural properties of the system.

3.2. Structural properties

Figure 4 shows the global pair correlation function $g(r)$ for various doses. The functions corresponding to doses of 0.18 DPA and 0.2 EPA reveal features similar to that of the quenched liquid. The Ni–Ni, Zr–Zr and Ni–Zr partial pair correlation functions (not shown

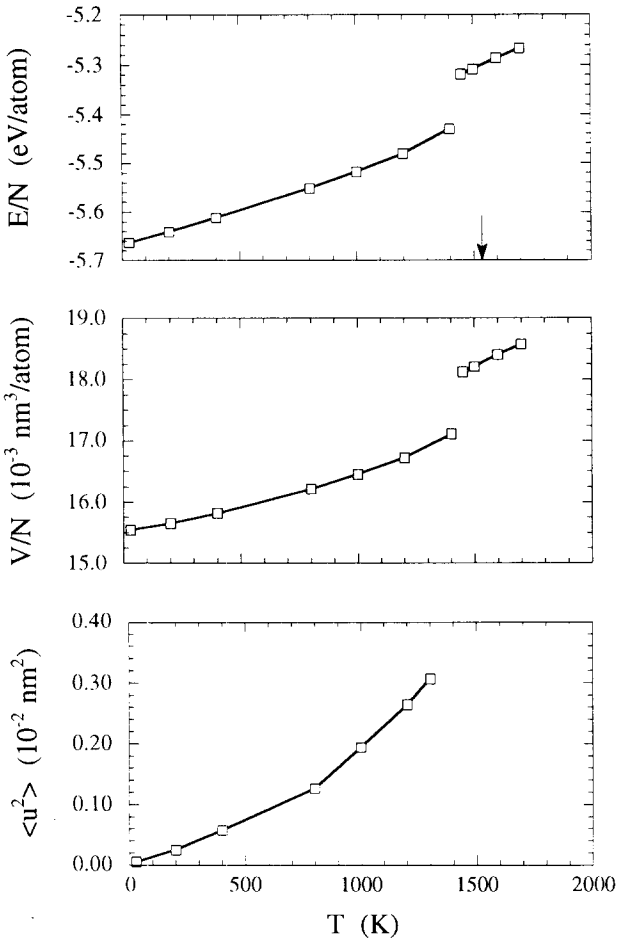

Fig. 2. The changes in the potential energy E/N per atom, the volume V/N per atom and the mean square displacement $\langle u^2 \rangle$ in NiZr as functions of temperature. The melting point is about 1400 K. The experimentally measured melting point is indicated by the arrow.

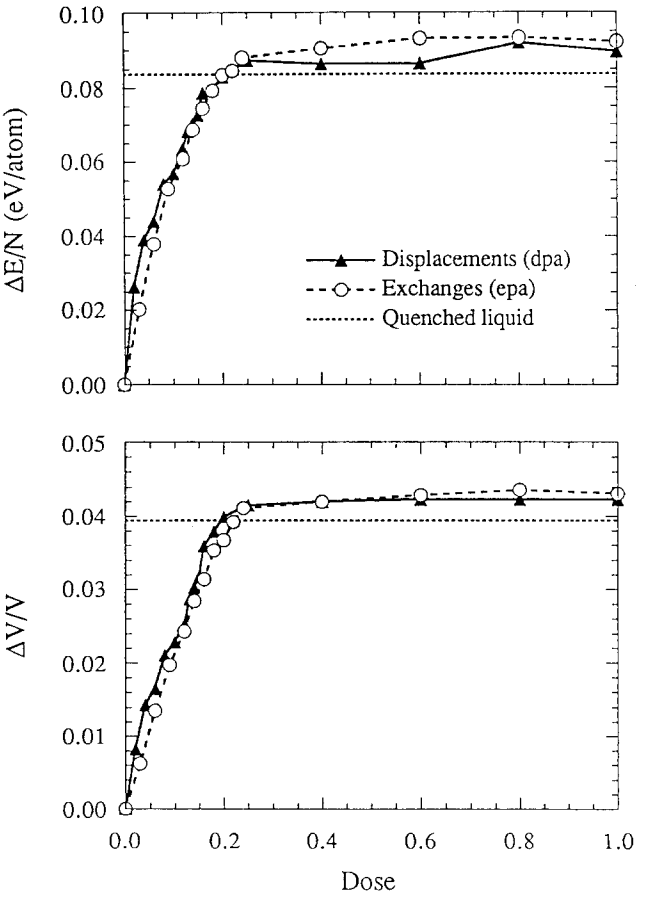

Fig. 3. The changes in the potential energy per atom and the volume expansion of the compound NiZr as functions of dose. The dotted lines indicate the values for the system quenched from 4000 K to 30 K.

here) were also calculated. The changes in these functions were similar to the changes in the global $g(r)$. It has been shown by Sabochick and Lam [9] in NiTi that the system may not be amorphous even when $g(r)$ exhibits features characteristic of the quenched liquid. The structure factor is considered to be a more reliable indicator of the system structure. The structure factor is given by

$$H(k) = \frac{1}{N^2} \left| \sum_{j=1}^{N} \exp\left[2\pi i (\boldsymbol{k} \cdot \boldsymbol{r}_j) \right] \right|^2 \tag{7}$$

where $\boldsymbol{r}_j$ is the position of atom j and $\boldsymbol{k}$ is the reciprocal lattice vector. $H(k)$ was calculated for various doses along three $\boldsymbol{k}$ vectors, namely [001], [100] and [101], and is shown in Fig. 5. $H(k)$ is characteristic of an amorphous material after 0.18 DPA. For the case of exchanges, the [002] peak can still be seen after 0.2 EPA. However, $H(k)$ for 0.4 EPA is identical to that of the quenched liquid. This indicates that NiZr can be amorphized by chemical disorder as well as Frenkel pairs and that the critical dose is smaller for the case of displacements. The long-range order parameter S was calculated as a function of the exchange dose to determine the order parameter prior to the start of amorphization. The order parameter for NiZr is defined as

$$S = 2f - 1 \tag{8}$$

where f is the fraction of Ni atoms on Ni lattice sites. Figure 6 shows that S decreases monotonically with increasing dose from a value of 1.0 for the perfect crystal to about 0.56 for a dose of 0.16 EPA. S was not calculated for doses above 0.16 EPA because the loss of topological order was considerable. Thus, amorphization occurs at $S \approx 0.56$. Further information about the atomic arrangement in real space can be obtained by projecting the atomic positions on the (100) plane as shown in Fig. 7. A loss of crystalline order can be visualized for a dose of 0.2 DPA.

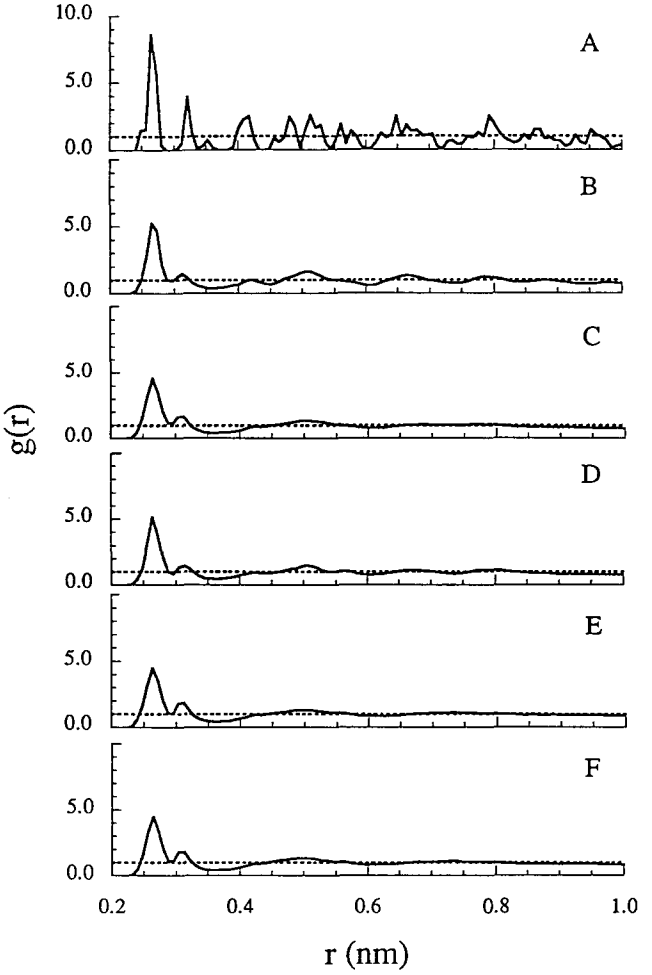

Fig. 4. The global pair correlation function $g(r)$ of NiZr for the following configurations at 30 K: curve A, perfect lattice; curve B, after 0.12 EPA; curve C, after 0.2 EPA; curve D, after 0.12 DPA; curve E, after 0.2 DPA; curve F, quenched liquid.

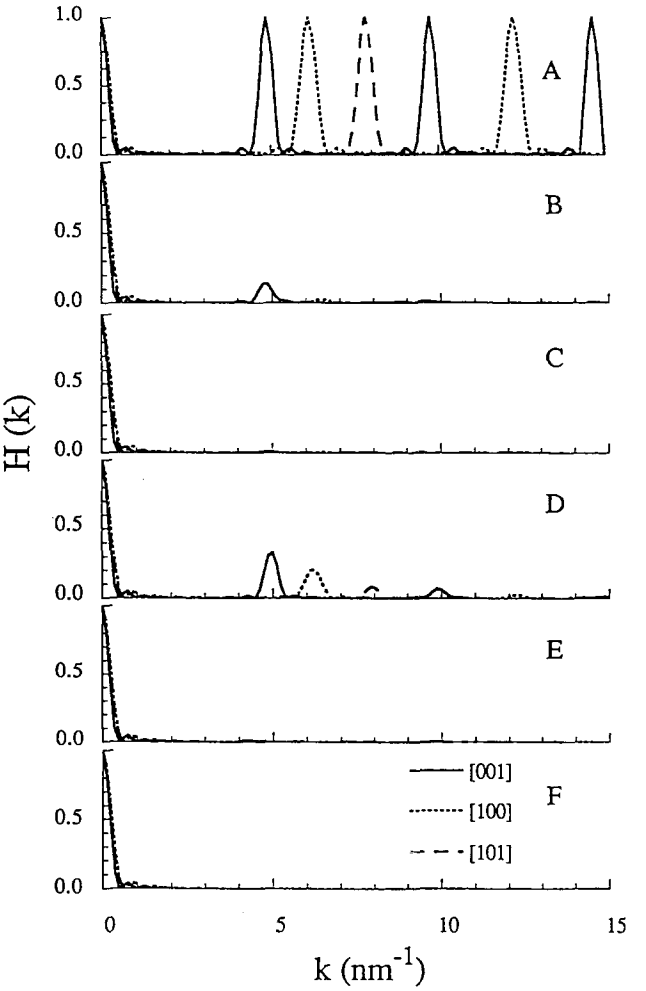

Fig. 5. The structure factor $H(k)$ of NiZr for the following configurations: curve A, perfect crystal; curve B, after 0.2 EPA; curve C, after 0.4 EPA; curve D, after 0.12 DPA; curve E, after 0.2 DPA; curve F, quenched liquid.

3.3. Mechanical properties

It has been suggested by Rehn *et al.* [26] and Okamoto *et al.* [27] that a softening of the shear modulus, suggestive of a mechanical instability, is a characteristic feature of compounds that are amorphized by irradiation. Dramatic softening by about 50% in the average shear elastic constant has been observed in Zr_3Al irradiated with 1 MeV Kr^+ [26, 27] and Nb_3Ir irradiated with α particles [28]. It is, therefore, of interest to study the changes in the shear moduli as a function of dose. We have performed such a study using the approach of Ray *et al.* [29] to calculate the elastic constants C_{44} and C'. In our case, C_{44} denotes the average of C_{44}, C_{55} and C_{66} while C' is given by

$$C' = \frac{C_{11}+C_{22}+C_{33}-(C_{12}+C_{23}+C_{13})}{6} \qquad (9)$$

Figure 8 shows the values of C_{44}, C' and their average C_{avg} as functions of exchange and displacement dose.

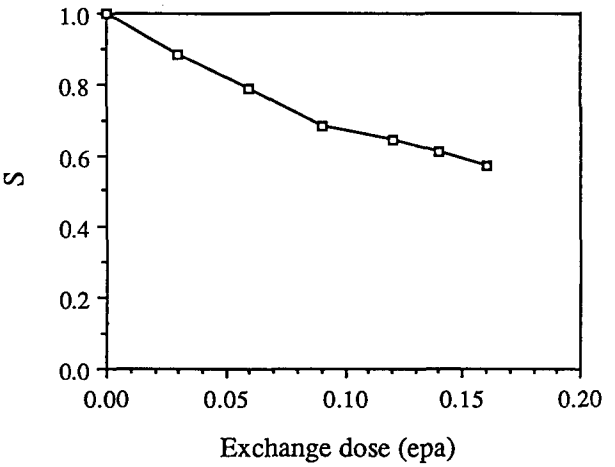

Fig. 6. The long-range order parameter of NiZr as a function of the number of exchanges per atom.

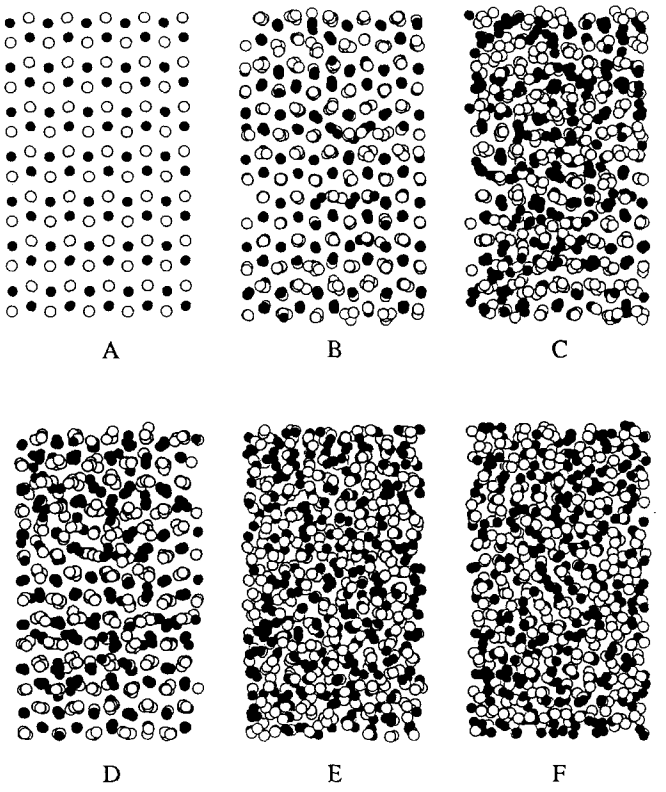

Fig. 7. Projections of the atomic positions on the (100) plane of NiZr, obtained from the following configurations: A, perfect lattice; B, after 0.12 EPA; C, after 0.2 EPA; D, after 0.12 DPA; E, after 0.2 DPA; F, quenched liquid.

In both cases C_{44} and C' decrease drastically with dose and become equal at 0.2 EPA or 0.2 DPA. When the dose is increased further, these quantities remain practically constant. The average elastic constant decreases from its value of 0.54 Mbar in the perfect crystal to about 0.23 Mbar at a dose of 0.2 DPA. The fact that the shear elastic constants become isotropic supports the evidence from the structural properties, *i.e.* NiZr can be amorphized by chemical disorder as well as by Frenkel pairs.

3.4. Defect energetics

The role played by chemical disorder in the present work is different from that reported in the Cu–Ti system [8, 10]. In order to understand the reasons for this difference, we have investigated the energetics of formation of antisite defects and Frenkel pairs using techniques described by Shoemaker *et al.* [30]. Sabochick and Lam [8] have reported energies of formation of 0.38 eV and 2.79 eV for an antisite defect and a Frenkel pair respectively in CuTi. We have found the corresponding energies in NiZr to be 2.18 eV and 2.59 eV. Since the antisite defect energy is considerably higher in NiZr than in CuTi, chemical disorder is more likely to cause amorphization in NiZr. The difference between the energies of formation of these two defects is also considerably smaller in NiZr. This could explain the similarity in the behavior of the thermodynamic properties of NiZr after exchanges and displacements. In addition, since the Frenkel pair energy is slightly greater than the antisite defect energy in NiZr, amorphization occurs at a slightly smaller dose with displacements.

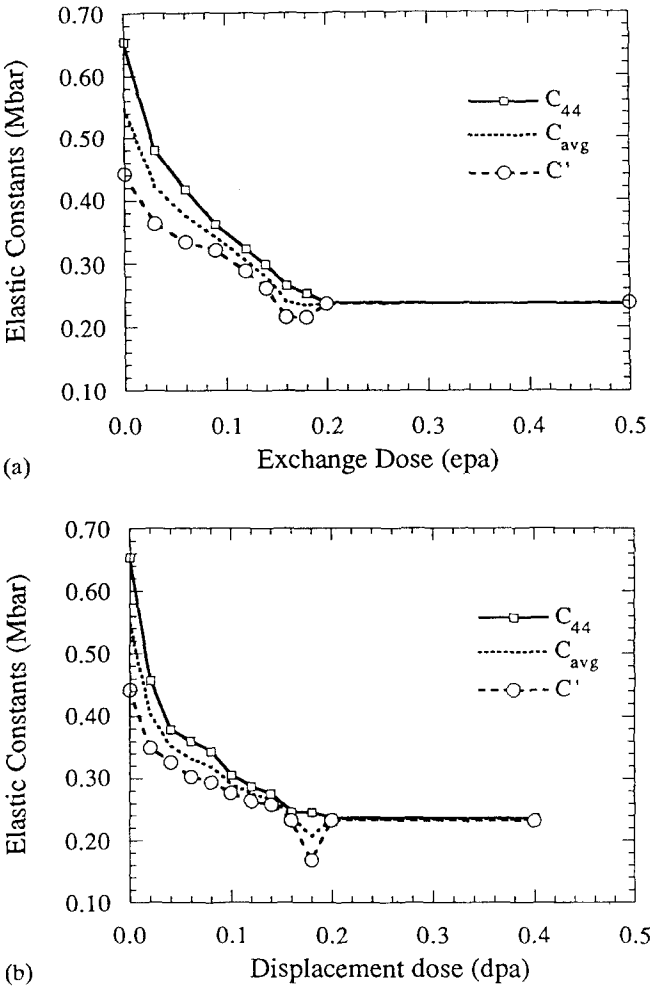

Fig. 8. The shear elastic constants of NiZr as functions of (a) the exchange dose and (b) the displacement dose.

4. Conclusions

We have used MD simulations in conjunction with embedded-atom potentials to study the electron-irradiation-induced amorphization of the compound NiZr. The energy and volume of the system rose above the corresponding quantities of the quenched liquid following both chemical disorder as well as the introduction of Frenkel pairs. The pair correlation function, structure factor and atom projections indicated that NiZr can indeed be amorphized by either of these processes. Amorphization occured at a critical dose of about 0.2 DPA. Prior to amorphization, the long-range order

parameter decreased monotonically to about 0.56. The average shear elastic constant dropped dramatically by about 60% at the critical dose and subsequently remained constant when the system had been completely amorphized.

These results show that it is possible to bring about solid state amorphization in NiZr by chemical disorder alone. Viewed in the light of the simulational study of the Cu–Ti system [8, 10], our work suggests that the nature of the driving force for electron-irradiation-induced amorphization varies from compound to compound. The energetics of antisite defect formation indicates that NiZr is a more likely candidate than CuTi for amorphization by chemical disordering. The behavior of the shear elastic constants is another interesting outcome of this study. The attainment of isotropy by the shear elastic constants can be used in simulational studies as an indication of complete amorphization.

The results of this simulation are in general agreement with the experimental observations of Xu *et al.* [12]. Xu and coworkers irradiated NiZr with 1 MeV electrons in the temperature range 10–120 K. They were able to amorphize NiZr at a critical dose of less than 0.4 DPA. They also found that the long-range order parameter decreased to about 0.5 prior to the onset of amorphization. The changes in thermodynamic properties with temperature and the ability of chemical disorder to amorphize the system are consistent with the results obtained by Massobrio *et al.* [11] in a simulational study of $NiZr_2$. The dramatic decrease in shear elastic constants observed in this work is in good accord with experimental observations of elastic softening prior to amorphization [26–28]. This indicates that a decrease in the elastic moduli might be a general feature of amorphization.

Acknowledgments

This work is supported by US Department of Energy, BES Materials Sciences, under Contract W-31-109-Eng-38, and National Science Foundation, under Grant DMR-8802847. It has benefited from a grant of time on the Cray computers at NERSC, Lawrence Livermore National Laboratory. One of the authors (R.D.) would like to thank Larry Rudsinski of the Computing and Telecommunications Division, Argonne National Laboratory, for his invaluable help with the vectorization of the DYNAMO code.

References

1 P. R. Okamoto and M. Meshii, in H. Wiedersich and M. Meshii (eds.), *Science of Advanced Materials,* ASM, Metals Park, OH, 1990, p. 33.
2 D. E. Luzzi, H. Mori, H. Fujita and M. Meshii, *Acta Metall., 34* (1986) 629.
3 D. E. Luzzi and M. Meshii, *Res. Mech., 21* (1987) 207.
4 H. Mori and H. Fujita, *Jpn. J. Appl. Phys., 21* (1982) L494.
5 H. Mori, H. Fujita and M. Fujita, *Jpn. J. Appl. Phys., 22* (1983) L94.
6 D. F. Pedraza, *J. Mater. Res., 1* (1986) 425.
7 J. Koike, P. R. Okamoto, L. E. Rehn and M. Meshii, *Metall. Trans. A, 21* (1990) 1799.
8 M. J. Sabochick and N. Q. Lam, *Phys. Rev. B, 43* (1991) 5243.
9 M. J. Sabochick and N. Q. Lam, *Mater. Res. Soc. Symp. Proc., 201* (1991) 387.
10 N. Q. Lam, P. R. Okamoto, M. J. Sabochick and R. Devanathan, *J. Alloys Comp., 194* (1993) 429.
11 C. Massobrio, V. Pontikis and G. Martin, *Phys. Rev. B, 41* (1990) 10486.
12 G. Xu, P. R. Okamoto and L. E. Rehn, *J. Alloys Comp., 194* (1993) 401.
13 M. S. Daw, M. I. Baskes and S. M. Foiles, personal communication, 1986.
14 D. J. Oh and R. A. Johnson, *J. Mater. Res., 3* (1988) 471.
15 J. H. Rose, J. R. Smith, F. Guinea and J. Ferrante, *Phys. Rev. B, 29* (1984) 2963.
16 C. J. Smith (ed.), *Metals Reference Book,* Butterworths, London, 5th edn., 1976.
17 B. D. Cullity, *Elements of X-Ray Diffraction,* Addison-Wesley, Reading MA, 2nd edn., 1978.
18 R. W. Siegel, in P. G. Coleman, S. C. Sharma and L. M. Diana (eds.), *Positron Annihilation,* North-Holland, Amsterdam, 1982, p. 351.
19 G. Simmons and H. Wang, *Single Crystal Elastic Constants and Calculated Aggregate Properties: A Handbook,* Massachusetts Institute of Technology, Cambridge, MA, 1971.
20 M. J. Sabochick and N. Q. Lam, to be published.
21 M. E. Kirkpatrick, D. M. Bailey and J. F. Smith, *Acta Crystallogr., 15* (1962) 252.
22 C. Becle, B. Bourniquel, G. Develey and M. Saillard, *J. Less-Common Met., 66* (1979) 59.
23 J. C. Gachon and J. Hertz, *Calphad, 7* (1983) 1.
24 F. R. Eshelman and J. F. Smith, *J. Appl. Phys., 46* (1975) 12.
25 P. Nash and C. S. Jayanth, *Bull. Alloy Phase Diagrams, 5* (1984) 144.
26 L. E. Rehn, P. R. Okamoto, J. Pearson, R. Bhadra and M. Grimsditch, *Phys. Rev. Lett., 59* (1987) 2987.
27 P. R. Okamoto, L. E. Rehn, J. Pearson, R. Bhadra and M. Grimsditch, *J. Less-Common Met., 140* (1988) 231.
28 M. Grimsditch, K. E. Gray, R. Bhadra, R. T. Kampwirth and L. E. Rehn, *Phys. Rev. B, 35* (1987) 883.
29 J. R. Ray, M. C. Moody and A. Rahman, *Phys. Rev. B, 32* (1985) 733; *33* (1986) 895.
30 J. R. Shoemaker, R. T. Lutton, D. Wesley, W. R. Wharton, M. L. Oehrli, M. S. Herte, M. J. Sabochick and N. Q. Lam, *J. Mater. Res., 6* (1991) 473.